A state of art review on methodologies for heat transfer and energy flow characteristics of the active building envelopes

Shukla, A, Liu, S & Wang, Y

Original citation:
Shukla, A, Liu, S & Wang, Y 2017, 'A state of art review on methodologies for heat transfer and energy flow characteristics of the active building envelopes' *Renewable and Sustainable Energy Reviews*, vol 78, pp. 1102-1116
http://dx.doi.org/10.1016/j.rser.2017.05.015

DOI 10.1016/j.rser.2017.05.015
ISSN 1364-0321

Publisher: Elsevier

Renewable and Sustainable Energy Reviews 78 (2017) 1102–1116

Contents lists available at ScienceDirect

Renewable and Sustainable Energy Reviews

journal homepage: www.elsevier.com/locate/rser

A state of art review on methodologies for heat transfer and energy flow characteristics of the active building envelopes

Yang Wang, Ashish Shukla*, Shuli Liu

School of Energy, Construction and Environment, Faculty of Engineering, Environment and Computing, Coventry University, CV1 2HF Coventry, UK

ARTICLE INFO

Keywords:
Active building envelope
Transpired solar collector
Heat transfer
Thermal efficiency
Turbulence model
Parametric analysis

ABSTRACT

Significant share of total final energy use is accounted by the building sector in most of the countries around the world. One way to reduce building energy consumption is to adopt energy efficiency technologies and strategies. Due to environmental concerns and high cost of energy in recent years there has been a renewed interest in building energy efficiency and integration of renewable energy technologies. Active building envelope technology, i.e. transpired solar collectors (TSCs), provides a cost-efficient way of minimizing energy demand of buildings in accordance with global principle of sustainability, which has also proven reliable for diverse applications such as preheating fresh air delivery into the buildings and supplying domestic hot water in summer etc. The objective of this paper is to review the heat transfer and energy flow characteristics of the active building envelopes, particularly focusing on various types of TSCs. Present work consists of background and concept of TSCs, research literature for thermal performance, theoretical modelling, experimental study and numerical simulation investigation. Diverse mathematical models, including thermal models, air flow models, porosity models, and turbulence models etc., have also been presented and compared. Following that, more than 20 parameters affecting TSC performance have been analyzed and evaluated. The literature has illustrated that the best overall performance of turbulence model is RNG k-ε; the effects of those parameters on TSC efficiency are completely different, depending on local climatic conditions, time and site constraints, and the interaction between different factors.

1. Introduction

Nowadays, the building sector accounts for approximately 40% of the total world final energy consumption and for about one third of CO_2 emissions into the atmosphere, which can result in global warming and climate changes [1,2]. Similarly, in the UK, the domestic sector is responsible for almost 40% of national carbon emissions [3]. The "Climate Change Act 2008" has already set a target of 80% reduction in CO_2 emissions in the UK (relative to 1990 emissions) to be achieved by 2050 [4]. The increasing trend towards building consumption will persist in the coming years due to the extension of built regions and related energy demands [2,5].

The building envelope plays a vital role not only in thermal comfort but also in building energy efficiency. There are significant opportunities for the building envelope to solve the aforementioned problems, which could exploit solar energy through integrating solar thermal technologies into the buildings. Transpired solar collector (TSC) is one of most popular solar thermal technologies, which is also called as active building envelope [6,7] from the perspective of TSC's active generation of solar thermal energy.

Research on TSCs started in the early 1990s [8,9] and was focused on feasibility studies and testing [10,11]. Authors (Shukla et al., 2012) have reviewed the performance of TSCs from the literature before 2012 [12]. In this work, the objective mainly focuses on the heat transfer and energy flow characteristics of TSCs for the recent five years, i.e., from 2012 to 2016, and those literatures were not reviewed by current authors before 2012 [14–43,46,49–54,56–62]. In Section 2, background and concept of active building envelopes will be introduced; in Section 3, the heat transfer and energy flow characteristics of the active building envelopes from the perspective of mathematical modelling,

Abbreviations: BIPV/T, Building-integrated photovoltaic-thermal; BPSC, Back-pass solar collector; CFD, Computational fluid dynamics; CHTC, Convective heat transfer coefficient; D, Diameter; EPSRC, Engineering and Physical Sciences Research Council; GTC, Glazed transpired collector; HEE, Heat exchanger effectiveness; IR, Infrared spectroscopy; P, Pitch; PIV, Particle image velocimetry; PV/T, Photovoltaic/Thermal; RANS, Reynolds-averaged Navier-Stokes; RMSE, Root mean square error; RNG, ReNormalization group methods; RSM, Reynolds Strees Model; SST, Shear Stress Transport; STC, Standard test condition; TI, Turbulence Intensity; TSC, Transpired solar collector; TTC, Transparent transpired collector; UTC, Unglazed transpired collector

* Corresponding author.
E-mail address: ashish.shukla@coventry.ac.uk (A. Shukla).

http://dx.doi.org/10.1016/j.rser.2017.05.015
Received 20 September 2016; Received in revised form 23 April 2017; Accepted 4 May 2017

Nomenclature

A_c	effective area of the collector in m^2
A_h	area of the holes in m^2
A_{PV}	total PV area in m^2
C_f	conversion factor (thermal to mechanical) and given as 0.2
C_p	specific heat capacity of air in J/kgK
D	perforation/hole equivalent diameter in m
F_{pb}	view factor between the UTC plate and the back wall
F_R	heat removal factor
G	incident solar irradiance on the UTC plate per unit area in W/m^2
h	convective heat transfer coefficient in W/m^2K
H	total height of UTC-2stage in m
H_u	UTC height in m
i	control volume index
k	air thermal conductivity in W/mK
N_h	holes number
Nu_x	Nusselt number (= hx/k)
P	hole pitch in m, i.e., distance between center of hole and center of next closest hole
ΔP	pressure drop in Pa
P_{PV}	electrical energy generated by PV panels in W/m2
Pr	Prandtl number (=α/υ)
Q	air volume flow rate in m^3/h
Q_{conv}	convective heat flux between difference surfaces (or air) in W/m2
Q_{gain}	thermal heat gain from the collector in W
Q_{rad}	radiative heat flux between different surfaces in W/m2
Q_{solar}	solar radiation absorbed by the plate (or PV module) in W/m2
q_u	heat collected from the collector in W
Re_x	Reynolds number (= vx/υ) where v is relevant velocity scale
T_{amb}	ambient temperature in K or °C
T_c	cavity exit air temperature in K
$T_{collector}$	collector temperature in °C
T_{in}	inlet temperature in K or °C
T_{out}	outlet temperature in K or °C
T_p	UTC plate surface temperature in K
T_{ref}	surface temperature of PV module under STC in K
T_s	air temperature through the perforation in K
T_{sky}	sky temperature in K
T_{sun}	sun temperature in K
U_L	overall heat loss coefficient in W/m2K
V_{suc}	mean surface suction velocity in m/s
V_{win}	air flow free-stream velocity or wind speed in m/s
W_{el}	electrical power in W
W_{fan}	fan power in W
W_{pc}	PV power in W
$W_{thermal}$	thermal power in W
x_n	hole spacing along flow path in mm

Greek symbols

α	air thermal diffusivity in m^2/s
β_{ref}	temperature coefficient of the PV module in %/K.
ε	effectiveness ratio of collector
ε_b	emissivity of the back wall
ε_p	emissivity of the UTC plate (PV panel)
η_c	efficiency of the TSC in %
η_{ci}	instantaneous efficiency of the BPSC in %
η_{ef}	effective efficiency in %
η_{et}	equivalent thermal efficiency in %
η_{fl}	first law efficiency in %
η_{pm}	fan motor efficiency in %.
η_{PV}	electrical efficiency for PV panels in %
$\eta_{PV/T}$	combined thermal and electrical efficiency for BIPV/T systems in %
η_{sl}	second law efficiency in %
η_{Tref}	electrical efficiency of PV module under STC in %
τ_α	effective transmittance-absorptance factor
σ	Stefan-Boltzmann constant (5.67×10^{-8} $W/(m^2K^4)$)
σ_p	plate porosity
υ	air kinematic viscosity in m^2/s
ξ	porosity of the TSC plate

experimental study, numerical simulations particularly CFD, and parametric sensitivity analysis including more than 20 parameters affecting TSC performance are indicated in detail, respectively; finally, conclusions and future work are drawn in Section 4.

2. Background and working principle for TSC

Active building envelopes, i.e., TSCs derived from Canada and USA and research on TSCs started in approximately early 1990s. TSCs have been already widely employed in USA and Canada and the technology has been extensively monitored by their government agencies. In addition, Natural Resources Canada has developed a feasibility tool called RETScreen to model the energy savings from TSCs [13]. However, TSCs are relatively new for other regions e.g. Europe and China.

Authors already described the historical development and working principle of TSCs, collector construction and its parameters, diverse types of TSCs in detail [12]. In this work, all those aforementioned contents will be not introduced again. The concept of TSCs is just presented using schematics below (Fig. 1(a)). There have already been some TSCs (active building envelop) applied in the existing buildings below (Fig. 1(b-d)).

Solar energy is employed by TSCs to heat the perforated absorber surface, which could transfer thermal energy to the ambient air for preheating fresh air delivered into buildings/room. Generally, the perforated absorber plate is a metallic sheet e.g. steel or aluminium, which could be integrated to the building façade and PV panels, and could generate solar thermal energy actively. Therefore, TSCs are also called as active building envelopes as mentioned before [6,7].

3. Heat transfer and energy characteristics of TSCs

Investigations on TSCs for the heat and airflow mass transfer, thermal efficiency, heat exchange efficiency, exergy efficiency, energy characteristics have been carried out for lots of researchers in last approximately 30 years, i.e., since 1991. Authors have already reviewed thermal performance of TSCs from the literature before 2012 [12]. In this work, a detailed summary for various models and study in recent 5 years has been presented in chronological order as shown in Table 1.

There are four different investigation methodologies for thermal performance of TSCs as follows:

1) Mathematical modelling study;
2) Physical experimental study including PIV, IR, prototype experiments and monitoring;
3) Numerical simulations including computational fluid dynamics (CFD); and
4) Parametric sensitivity studies.

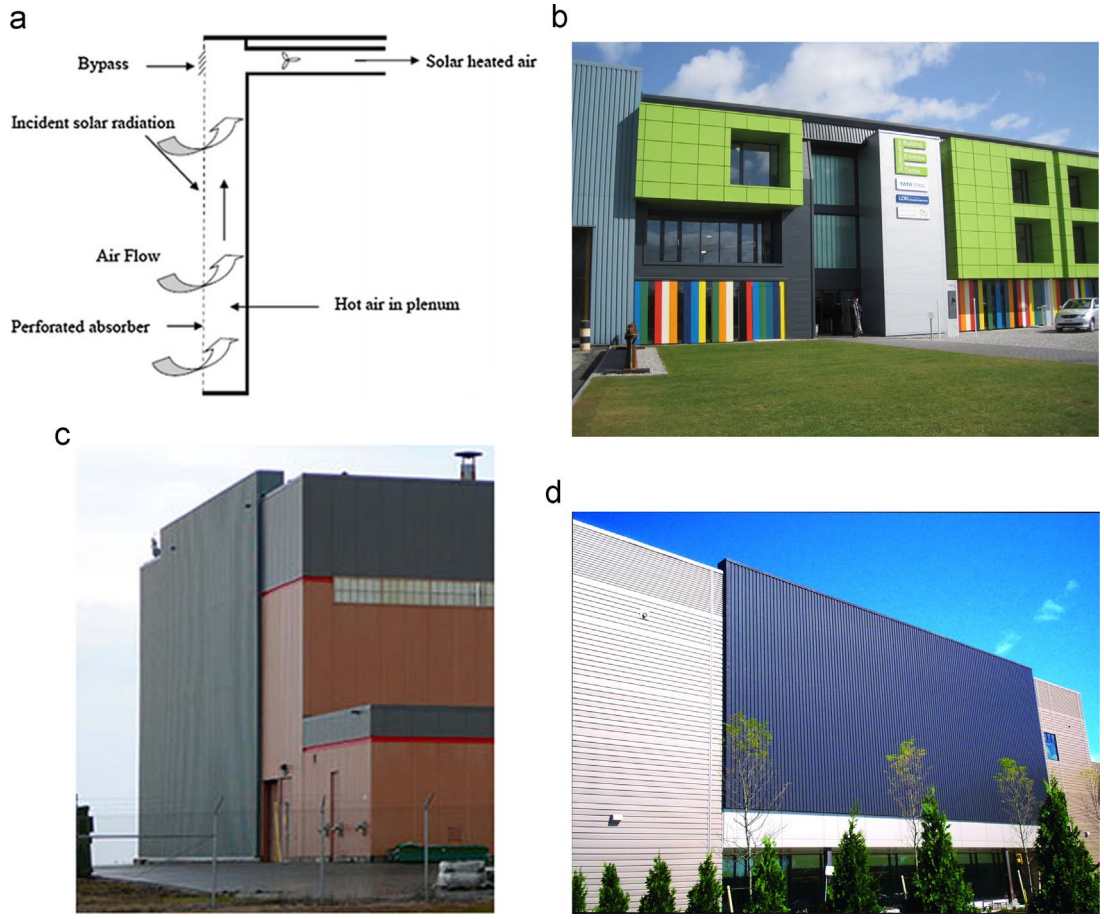

Fig. 1. (a) Schematics of standalone transpired solar collector [12]**. (b)** Examples of active building envelope system in the existing buildings: Sustainable Building Envelope Centre UK. **(c)** US Military Army Building. **(d)** Sherwood Middle School, Massachusetts, US.

Seen from the Table 1, there are mainly two types of transpired solar collectors (TSCs) classified by their materials including unglazed transpired collector (UTC), and glazed transpired collector (GTC) or called transparent transpired collector (TTC). According to the metal sheets pattern of solar collector system, it includes flat and corrugated TSCs. In addition, TSCs could be also categorized by their configuration as follows: stand-alone TSC, hybrid and building integrated TSC [12].

3.1. Mathematical models for heat transfer study

3.1.1. Thermal modelling of TSC system

Several mathematical/thermal model for TSC has been currently reported in literature. This section categories them in three main areas (i) energy balance (ii) efficiency calculations/models (iii) heat exchange effectiveness and (iv) Nusselt Number. A developed optimal BIPV/T system with UTC has been investigated analytically, experimentally and numerically [14,18,22,23]. Its thermal network of UTCs with and without PV modules is illustrated schematically in Fig. 2.

The cavity underneath the UTC plate is separated into several control volumes (e.g. *i*, *i+1* etc.). One corrugation is corresponded to each control volume. The energy (heat) balance analysis was carried out on each temperature node of every control volume, which will be discussed in the following Section Energy balance.

(i) ***Energy balance*** (Heat balance)

Energy balances at the UTC surface (heat transfer surface), the air node in the cavity and the surface of the back wall were defined by Li et al. [14], which also reflect the heat balances of the UTC plate and the air fluid [16], using the Gauss-Seidel method as

$$Q_{solar} = Q_{rad\_p\_sky} + Q_{rad\_p\_b} + Q_{conv\_p\_a} + Q_{conv\_p\_c} \quad (1)$$

$$Q_{conv\_p\_c} = (i - 1)\rho V_{suc} C_p (T_{c\_i} - T_{c\_i-1}) + \rho V_{suc} C_p (T_{c\_i} - T_s) + Q_{conv\_c\_b} \quad (2)$$

$$Q_{rad\_p\_b} + Q_{conv\_c\_b} = 0 \quad (3)$$

where Q_{solar} is the solar radiation absorbed by the UTC plate in W/m^2. $Q_{rad\_p\_sky}$ and $Q_{rad\_p\_b}$ represent the radiation exchange between the plate and the sky, and the back wall, respectively, which can be calculated as in Eqs. (4) and (5):

$$Q_{rad\_p\_sky} = \varepsilon_p \sigma (T_{p\_i}^4 - T_{sky}^4) \quad (4)$$

$$Q_{rad\_p\_b} = \sigma F_{bp} \left(\frac{1}{\varepsilon_p} + \frac{1}{\varepsilon_b} - 1 \right)^{-1} (T_{p\_i}^4 - T_{b\_i}^4) \quad (5)$$

$Q_{conv\_p\_a}$, $Q_{conv\_p\_c}$ and $Q_{conv\_c\_b}$ are the convective heat flux between the plate and ambient air, and cavity exit air, between cavity exit air and the back wall, respectively, in W/m^2. V_{suc}, i, C_p, T_c, T_s, T_p, T_{sky}, σ, F_{pb}, ε_b, ε_p are the mean suction velocity in m/s or m^3/(s*m^2), control volume index, specific heat capacity of air in J/kgK, cavity exit air temperature, air temperature through the perforation, UTC plate surface temperature and sky temperature in K, Stefan-Boltzmann constant (5.67×10^{-8} W/(m^{2}K^4)), view factor between the UTC plate and the back wall, emissivity of the

Table 1
Summary table for various models and study reported in literature from 2012 to 2016.

Publications/ References	Objectives and Method Used	Type of TSCs	Software/ Model Used	Conclusions	Special Findings
Li et al. 2014 [14]	To predict cavity exit air temperature, plate surface temperature with Weather and design parameters; Gauss-Seidel method for energy prediction of UTCs with and without PV modules	Corrugated UTCs/ UTCs integrated with BIPV/T	CFD, Correlation prediction, Physical experiment, design concept of PV module dimensions	Regression predictions illustrate a good agreement with the CFD simulation results, with 90% of the prediction points within ± 20% error band for both Nu correlations and within ± 10% error band for the effectiveness.	The portion of the exterior heat flux recaptured by suction should be considered. The model can capture the trends and peaks very well.
Li et al. 2016 [15]	To investigate the heat transfer and flow resistance characteristics of a vacuum glazed TSC with slit-like perforations; To analyze the effects of key parameters in relation to effective thermal efficiency considering fan power	GTC with slit-like perforations	Mathematical and Physical Experiment, Matlab−7: temperature of each control volume; Thermal modelling and pressure drop model	Perforation diameter and pitch have a minor impact on the heat collected compared to the pressure drop for the ranges of D and P.	Effective efficiency improves with increasing of perforation diameter and ambient temperature, decreasing of the pitch, plenum thickness and inlet air temperature; the effect of coating emissivity is less obvious than that of absorptivity.
Belusko et al. 2008 [16] (Not reviewed by Shukla et al. 2012)	To investigate the performance of jet impingement in USCs of roof	USCs	Mathematical and Physical Experiment	Jet impingement can enhance the thermal efficiency of collector by 21% and increase pressure losses a little. The efficiency can enhance with increasing of the hole spacing.	Jets' Flow distribution along the collector is the most important parameter to determine the efficiency.
Vasan et al. 2014 [17]	To study wind effects on UTCs	UTCs	Physical Experiment	Assumption of reference uniform wind speed through the UTC will cause up to 50% overestimation of heat exchange effectiveness (HEE) and up to 20% underestimation of convective heat transfer coefficients (CHTC), compared to realistic non-uniform distribution.	Winds with 45° incidence angle to the UTC have most significant impact on CHTC and HEE.
Li et al. 2014 [18]	To investigate important factors which affect the performance of corrugated UTCs with and without PV panels	Corrugated UTCs/UTCs integrated with BIPV/T	CFD	Horizontal installations of UTCs are proposed for low-rise buildings and vertical for high-rise buildings. The least significant factor on energy performance is amplitude, then crest length and cavity width. The wavelength and slope length have the most obvious effect on the collector temperature.	Thermal efficiency and cavity exit air temperature will decrease with increasing TI, particularly when increasing wind speed and decreasing suction velocity.
Croitoru et al. 2016 [19]	To prove the efficiency increase of lobed geometries, underlining the benefit of passive solar systems	UTCs	Physical Experiment (PIV, IR)	The more complex dynamics of the lobed flows, it causes a better heat transfer rate. The comparison between a conventional USC and a new geometry with innovative perforation will result in interesting results, with nearly 40% increase in heat transfer between the perforated cladding and the exhausted airflow.	The stream wise vortices induced by the lobed cross shaped perforation help in the stabilization of the jet flows inside the ventilated cavity.
Tajdaran et al. 2016 [20]	To develop a comprehensive CFD model for TSC systems	TSCs	CFD (STAR-CCM+) and experiment	Wind angles affect the impact of solar radiation on the operating temperature of TSCs. Effect of wind angle and solar radiation on Heat Change Effectiveness is minor.	Heat Exchange Effective ness is at its highest value when system works at the lowest suction ratio with lowest wind speed.
Badache et al. 2012 [21]	To model and optimize thermal performance of a UTC prototype using a full factorial experiment with four factors at three levels	UTC	Physical experiment	The resulting regression model shows the impact of hole diameter is not statistically significant (with > 95% certainty), while that of irradiation is.	The response surfaces made it possible to identify the optimal set of four parameters for which the UTC efficiency ranges between 70% and 80%.
Li et al. 2013 [22]	To analyze the convective heat transfer processes for both flat and corrugated UTCs	Corrugated UTCs	CFD	The suction velocity has the most obvious impact on the boundary layer development and thermal	The level of turbulence intensity is less important than the presence of perforations in the approach flow for flat UTCs.

(continued on next page)

Table 1 *(continued)*

Publications/ References	Objectives and Method Used	Type of TSCs	Software/ Model Used	Conclusions	Special Findings
				efficiency in UTCs compared to suction ratio; RNG k-ε model has the most accurate and consistent results with economic computing cost compared to Standard k-ε, SST k-ε, Realizable k-ε and RSM.	However, for corrugated UTCs, the perforation dimensions play a less significant role in the system performance than the incident turbulence intensity.
Collins et al. 2014 [24]	To evaluate the effectiveness in the asymptotic region and heat loss due to wind in the starting region of an unglazed transpired solar collector with a trapezoidal corrugation	Corrugated UTCs	CFD	In theory, wind velocity has no impact on the calculated heat exchanger effectiveness. Attached flows were seen to appear just for high suction velocities (0.03 and 0.04 m/s) and low wind speeds (0.5 m/s).	Heat transfer and absorber heat exchanger effectiveness are not the function of wind velocity.
Greig et al. 2012 [25]	To investigate experimentally flow dynamics in a channel with a corrugated surface in a TSC	Corrugated TSC	Physical experiment (PIV)	Strong turbulence occurs even at the Reynolds number lying within the conventional laminar domain.	Strong turbulence produced by the corrugation waveform and its effective diffusion throughout the channel could obviously improve the heat transfer from the corrugation wall and thermal performance of TSC.
Gholampour et al. 2016 [26]	To develop a predictive model, validate, and investigate the PV/Thermal flat transpired plate prototype capabilities	TSCs integrated with PV/T	CFD, Physical experiment	Increasing suction velocity will improve the first law efficiency but decrease the second law efficiency. It is not determined to obtain a unique optimum value for suction velocity or PV coverage percent because of their values relying on the solar radiation.	Increasing coverage percent of PC has a positive impact on the second law efficiency but a negative impact on the first law efficiency.
Badache et al. 2013 [27]	To investigate thermal efficiency of a UTC experimentally and numerically	UTCs	CFD, Physical experiment	Both Thermal efficiency of UTC and absorber plate effectiveness are relatively insensitive to the thickness of the plenum.	A Weak heat exchange process appears in the plenum: the maximum efficiency difference between the two plenum thickness (5 and 15 cm) is just 3.25%.
Greig et al. 2013 [28]	To examine the air flow behavior in the channel of TSC considering different heating conditions	TSC	Physical experiment (PIV)	Collector efficiencies up to 70% were found due to the corrugation surface geometry, which not only improved turbulence but also provided a larger heat transfer surface area.	Radiation heat transfer from the heated corrugation wall to the construction wall not only increased the construction wall temperature but also produced 15% – 25% of the total heat gain of the air.
Love et al. 2014 [29]	To evaluate the technical and economic feasibilities of a TSC duct to provide supplemental heating in a swine nursery and turkey brooder barn	TSC	Monitoring/ Physical Measurement	Barn CO_2, RH and temperature values were unaffected by TSC.	Short-term efficiencies were higher in the swine TSC (> 61%) and the turkey TSC (39–50%) probably due to the lower face velocity of the turkey TSC, which increased heat losses of TSC.
Gao et al. 2014 [30]	To develop a mathematical model for predicting thermal performance of GTC	UTC and GTC	Mathematical modelling, Matlab	Glazing of GTC could decrease convective heat losses caused by high crosswind velocities effectively, although it produces optical loss.	A huge amount of energy could be saved with the GTC application to space heating in cold climates.
Gao et al. 2013 [31]	To analyze heat transfer characteristic in UTC using CFD	UTC	CFD (Fluent 6.3)	Heat transfer is remarkably improved in UTC due to good synergy between velocity vector and temperature gradient, and the thermal efficiency of UTC is thus much higher than that of flat-plate collector.	Hole pitch effect on heat transfer in UTC is important, while hole diameter effect is less noticeable.
Badache et al. 2014 [32]	To investigate experimentally thermal performance of TTCs	TSC/TTCs	Physical experiment	The effect of interaction between plenum thickness and slot width on collector efficiency is the strongest.	Efficiency of the TTC is moderately affected by the plenum thickness.
Rad et al. 2016 [33]	To investigate the performance of UTC–2stage through developing mathematical model validated by experimental results	UTC	Physical experiment and mathematical modelling (Matlab 7.0)	Increasing solar radiation or hole diameter will causes the maximum equivalent thermal efficiency at a higher (H_u/H) value. However, the maximum equivalent thermal efficiency takes place at a lower (H_u/H) value with increasing the hole pitch, suction velocity and wind velocity.	Increasing suction velocity and wind velocity will causes the maximum second law efficiency at a lower (H_u/H) value; increasing the solar radiation will result in the maximum second law efficiency at a higher (H_u/H) value.
Paya-Marin et al. 2016 [38]	To develop a novel wall-integrated and unglazed solar air collector i.e. back-pass non-transpired solar collectors (BPSC)	UTC	Physical experiment	It can be achieved for the instantaneous efficiencies up to 39% with a combination of collector lengths and effective air flow rates in the	There is no effect on the performance of BPSC when wind speeds are up to 4 m/s across the collector metal plate.

(continued on next page)

Table 1 *(continued)*

Publications/ References	Objectives and Method Used	Type of TSCs	Software/ Model Used	Conclusions	Special Findings
Semenou et al. 2015 [39]	To present a simple model for thermal solar collectors to be employed in the design steps of an installation without the use of CFD simulations	TTC	Mathematical modelling, physical experiment	range of 90–120 $m^3/h/m^2$ The impact of external temperature on the temperature gain is slight.	The addition of a second intake on the solar collector could maintain high thermal efficiency in spite of operating conditions.

back wall and UTC plate.

For the case of with PV panels, it is similar to the above case of without PV panels. Energy balances at the surface of the PV module, the air node in the cavity and the surface of the back wall are written as

$$Q_{solar} = Q_{rad\_PV\_sky} + Q_{rad\_PV\_c} + Q_{conv\_PV\_a} + Q_{conv\_PV\_c} + P_{PV} \quad (6)$$

$$Q_{rad\_PV\_c} + Q_{conv\_PV\_c} = (i-1)\rho V_{suc} C_p (T_{c\_i} - T_{c\_i-1}) + \rho V_{suc} C_p (T_{c\_i} - T_s) + Q_{conv\_c\_b} + Q_{rad\_c\_b} \quad (7)$$

$$Q_{rad\_c\_b} + Q_{conv\_c\_b} = 0 \quad (8)$$

where P_{PV} is the electrical power generated by the PV panels in W/m^2. Each term calculation is similar to Eqs. (1)–(3), just using the thermal characterisitics of PV module instead of the characterisitics of the UTC plate. $Q_{rad\_PV\_c}$ and $Q_{rad\_c\_b}$ represent the radiation exchange between the PV module and UTC plate, as well as between the UTC plate and the back wall, respectively. Here noted that the temperature of UTC plate T_p is considered to be equal to the cavity air temperature T_c [40].

(ii) ***Efficiency***

a) *Collector efficiency*

The thermal efficiency of TSC [27,30,32,38], which is used as a measure of heat transfer performance for the TSC, is calculated from the ratio of the useful heat gain from the collector to the incident irradiance on the collector surface and could be determined as

$$\eta_c = [\dot{m}_{out} C_p (T_{out} - T_{amb})/A_c G]\% \quad (9)$$

where $\dot{m}_{out}$ is the mass flow rate through the TSC in kg/s, T_{out} is the outlet air temperature in °C, T_{amb} is the ambient temperature in °C, A_c is the effective area of the collector in m^2, G is the incident solar irradiance on the collector surface in W/m^2.

Badache et al. [32] put forward a novel formula of the collector efficiency as a function of air mass flow rate in the range of 2.2–6.3 g/s, which is written as:

$$\eta_c = 80.31 + 14.89\dot{m}_{out} - 7.66\dot{m}_{out}^2 \quad (10)$$

b) *Effective efficiency*

A novel efficiency defined by Gupta et al. [15,41] namely effective efficiency η_{ef} taking into account the fan power requirement arising from the airflow resistance via solar collector, which could be calculated by Eq. (11).

$$\eta_{ef} = \frac{\left[q_u - \left(\frac{W_{fan}}{C_f}\right)\right]}{A_c G} = \eta_c - \left[\frac{Q\Delta P}{\eta_{pm} C_f}\right]/3600 A_c G \quad (11)$$

where q_u is the heat collected from the collector in W, W_{fan} is the fan power in W, C_f is the conversion factor (thermal to mechanical) and given as 0.2, Q is the air volume flow rate in m^3/h, ΔP is the pressure drop in Pa, η_{pm} is the fan motor efficiency in % and given as 0.85. The effective efficiency presents the ratio of the net heat gain to the total solar energy input on the collector surface.

c) *First law efficiency (energy efficiency)*

The instantaneous first law or energy efficiency η_{fl} for TSC with PV/T system was defined by Gholampour et al. [26] as a ratio of the useful energy delivered to the received solar energy by the collector:

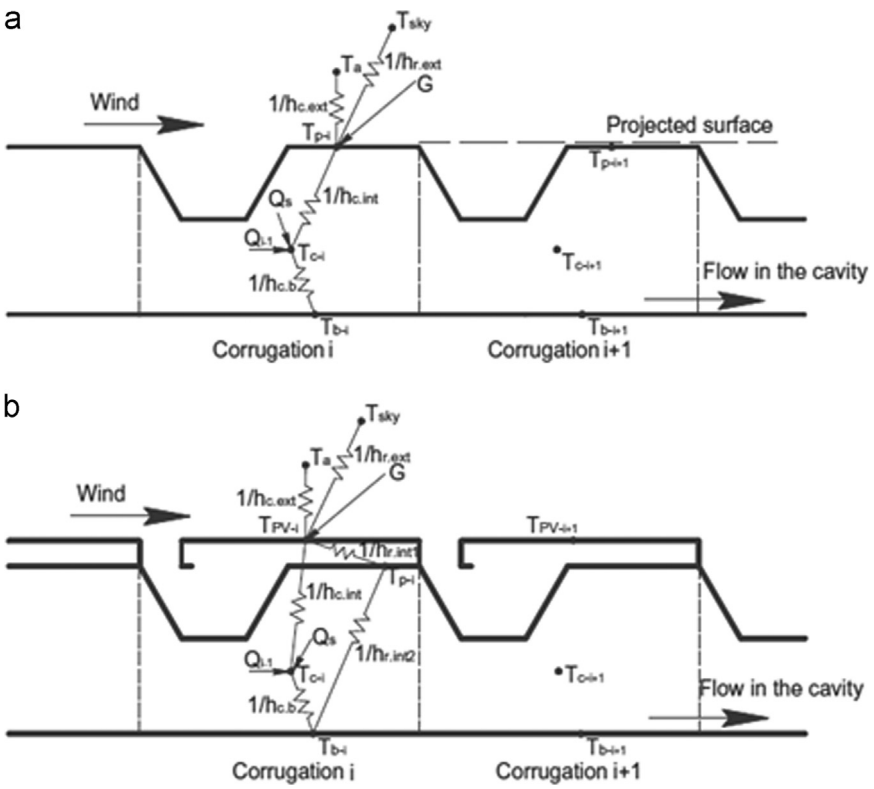

Fig. 2. Resolution algorithm instead of CFD methodology from Semenou et al. [39].

$$\eta_{fl} = (usefulenergy/receivedenergy)$$
$$= [\dot{m_{out}} C_p (T_{out} - T_{in}) + W_{pv} - W_{fan}]A_c \quad (12)$$

where W_{pv} is the power of PV panel in W, W_{fan} is the power of fan in W.

d) *Second law efficiency (exergy efficiency)*

Exergy analysis becomes more significant and helpful for a better design of TSC with PV/T system, since PV/Thermal flat transpired collectors generate both thermal and electrical energy. Similar to the first law definition, the second law efficiency η_{sl} [26,33,42,43] could be also written as:

$$\eta_{sl} = (usefulexergy/reveivedexergy)$$
$$= [\dot{m_{out}} C_p (T_{out} - T_{in} - T_{amb} ln (T_{out}/T_{in})) + W_{pv}]/A_c$$
$$G\left[1 - \left(\frac{4T_{amb}}{3T_{sun}}\right) + (1/3)(T_{amb}/T_{sun})^4\right] \quad (13)$$

where T_{sun} is the sun temperature, which is equal to approximately 6000 K. The second law efficiency represents a kind of the quality of useful energy gains, since the energy quality is very important for TSC with PV/T system [26].

e) *Equivalent thermal efficiency*

In order to evaluate the performance of TSC with PV/T system well, equivalent thermal efficiency η_{et} could be defined as the electrical-to-thermal ratio [26,33]:

$$\eta_{et} = W_{el}/W_{thermal} \quad (14)$$

where W_{el} is the electrical power in W and $W_{thermal}$ is the thermal power in W. Equivalent thermal efficiency is an very favorable tool or index for determining the optimum values of the key parameters e.g. suction velocity and PV coverage percent at various solar radiation intensity [26]. According to the renewable energy market, the value of electrical-to-thermal ratio i.e. equivalent thermal efficiency is considered as four [26,44]. From the perspective of the equivalent thermal efficiency, the optimum suction velocity value is 0.045 m/s at 400 W/m^2 and 0.06 m/s at 800 W/m^2, meanwhile, the optimum PV coverage percent is about 55% at 400 W/m^2 and around 45% at 800 W/m^2 [26].

f) *Instantaneous efficiency of the BPSC*

The instantaneous efficiency of the BPSC η_{ci} is defined by the equation of Hottel-Whillier-Bliss equation [38,45] and Eq. (14): efficiency of the TSC.

$$\eta_{ci} = \frac{[\dot{m_{out}} C_p (T_{out} - T_{in})]}{A_c G} = F_R \tau_\alpha - [F_R U_L (T_{in} - T_{amb})]/G \quad (15)$$

where $\dot{m}_{out}$ is F_R is the collector efficiency factor, τ_α is the effective transmittance-absorptance factor, U_L is the heat loss coefficient in W/m^{2}K, T_{in} is the inlet temperature in °C. For the term of the effective transmittance-absorptance product in the above Eq. (15) $F_R\tau_\alpha$, and the term of overall heat transfer coefficient for losses from the collector $F_R U_L$ are constant over the whole collector plane [38].

(i) ***Heat exchange effectiveness*** (HEE)

The HEE of the TSC could be defined as the air temperature rise in the collector to the maximum temperature rise [24,27,46]. There is another name for HEE i.e. the effectiveness ratio of collector [14,47], which was defined by Van Decker based on the plate surface temperature (T_p), the ambient temperature (T_{amb}), and air temperature through the perforation (T_s), which maintains relatively a constant along the plate, as follows:

$$\varepsilon = (T_s - T_{amb})/(T_p - T_{amb}) \quad (16)$$

HEE could be separated into three partials effectiveness (ε_f, ε_h and ε_b) combined each region in order to compare the temperature rise in the performation/hole, the front and back sides of the UTC:

$$\varepsilon_f = (T_{in,h} - T_{amb})/(T_p - T_{amb}) \quad (17)$$

$$\varepsilon_h = (T_{out,h} - T_{in,h})/(T_p - T_{amb}) \quad (18)$$

$$\varepsilon_b = (T_{out} - T_{out,h})/(T_p - T_{amb}) \quad (19)$$

where $T_{in,h}$ is the average air temperature at the slot inlet in °C, $T_{out,h}$ is the average air temperature at the slot outlet in °C. Following that, the total effectiveness could be expressed by:

$$\varepsilon = \varepsilon_f + \varepsilon_h + \varepsilon_b \quad (20)$$

(ii) **Nusselt number** (Nu)

In heat transfer at boundary (surface) within fluid, Nusselt Number is the ratio of convective to conductive heat transfer across (normal to) the boundary and this makes this parameter very relevant for TSC as it further includes diffusion within the surface/holes. *Nu* number could be estimated by an empirical correlation [15,48] as follows:

$$Nu_D = 2.75[(P/D)^{-1.2} Re_D^{0.43} + 0.011\sigma_p Re_D (V_{win}/V_{suc})^{0.48}] \quad (21)$$

where P is the pitch in m, D is the perforation equivalent diameter in m, Re_D is Reynolds number, σ_p is the plate porosity, V_{win} is the air flow free-stream velocity or wind speed in m/s, V_{suc} is the surface suction velocity in m/s.

However, *Nu* of convection between fluid and plate could be expected [16] as follows at very small hole diameters:

$$Nu_p = 0.17 + 0.725 Pr^{0.388} \sqrt{Rej}\, 40 \le Rej \le 2000 \quad (22)$$

where Pr is Prandtl number, Rej is based on the gap between the surfaces.

Collins et al. [24] obtained the *Nu* number for all flow based on fit analysis of the numerical data using a least square power law, which is written as:

$$Nu_p = 0.0081 Re_s^{2.0829} \quad (23)$$

where Re_s is the suction parameter and is equal to V_{win}/V_{suc}. The aforementioned correlation is just suitable for wind velocities in the range of 0.5–2 m/s, and suction velocities of 0.01–0.04 m/s.

Gholampour et al. [26] estimated Nu number for TSC plate and PV panel based on parameter studies as follows.

$$Nu_p = 0.7112 Re^{0.713} (a/b)^{-0.0337} (P/D)^{0.02188} \quad (24)$$

and

$$Nu_{pv} = 0.7145 Re^{0.5243} (a/b)^{-0.03003} (P/D)^{-0.01079} \quad (25)$$

where a/b is the width to length of PV panel ratio. The above correlation results for *Nu* number of TSC plate and PV panel have been compared with CFD numerical results.

3.1.2. Combination with electrical modelling of PV

The electrical efficiency of PV modules with UTC is generally defined as a function of its surface temperature and written as [14,49]:

$$\eta_{PV} = \eta_{Tref}[1 - \beta_{ref}(T_{PV} - T_{ref})] \quad (26)$$

where η_{Tref} is the electrical efficiency of module under STC (standard test condition) in %, T_{ref} is the surface temperature of PV module under STC in °C, β_{ref} is the temperature coefficient of the PV module in %/K. Following that, the electrical energy generated P_{PV} can be obtained as Eq. (27), which is a function of the incident solar irradiance G in W/m^2. The combined thermal and electrical efficiency for BIPV/T systems $\eta_{PV/T}$ can be written as Eq. (28).

$$P_{PV} = G\eta_{PV} \quad (27)$$

$$\eta_{PV/T} = [(Q_{gain} + P_{PV} A_{PV})/A_c G]\% \quad (28)$$

Q_{gain} is the thermal heat gain from the collector in W, A_{PV} and A_c are the total PV and collector effective area in m^2, respectively.

3.1.3. Resolution algorithm Vs CFD

Semenou et al. [39] presented a simple model for TSC to be employed in the design steps of an installation instead of CFD simulations at each step of the design, which calculates very fast and could reduce strongly the costs of expensive standard CFD simulation. Fig. 3 illustrates the resolution algorithm developed by them in detail in order to determine the temperature vectors.

Authors claimed that predicted thermal efficiencies of TSC are within 2% of discrepancy as provided by Solar Rating and Certification Corporation (SRCC). However, it is worth to note that results were validated only for small collector size of 4.5 m^2 and model may show further variations for large size TSC and other BIPV/TSC systems, which further need to be investigated.

3.1.4. Porosity model

In the study of TSC performance effective absorber area is calculated using porosity model. Porosity of any TSC might depend on hole patterns, distance between holes and size (diameter) of the holes. This factors plays a very important role as it directly determines the useful solar energy and effective absorber area and indirectly impacts on flow rate, plenum size, air flow and heat losses [12]. The porosity ξ could be defined as the ratio of the area of the holes A_h to the area of collector plate A_c [26]:

$$\xi = N_h A_h / A_c \quad (29)$$

where N_h is the holes number depending on the hole patterns. When the hole pattern is square, ξ could be formulated and simplified as [26,39,47]:

$$\xi = (\pi/4)(D/P)^2 = 0.78(D/P)^2 \quad (30)$$

When the hole pattern is triangle, ξ could be formulated and simplified as [26,48]:

$$\xi = 0.907(D/P)^2 \quad (31)$$

3.2. Experimental study

3.2.1. Experimental apparatus/setup

Corresponding to the configuration of active building envelope and its thermos-physical characteristics, the experimental system mainly involved the *TSC system element*: collector (absorber plate), metal profile, air duct, fan, PV modules [14], PCM; *Thermal apparatus*: pyranometer [27,29,38], IR [19], radiometer [15]; *Sensors or transduce* e.g. Pressure transducer/pressure transmitter [38], sensors of temperature: thermocouples (PT 100 probes [38]), thermistors [29,38]; *Air flow apparatus* including PIV [19,25,28], velocity meter, TSI wind speed tester [15], laminar flow element, hot-wire anemometer/anemonmetry [14,27,38,47] wind tunnel [17]; *Electrical devices*: solar simulator (incandescent lamps [16], halide lamp [19]), power resistor; *Data acquisition and analysis instrument*: Fluke [15] and Hobo data logger [29].

3.2.2. Aims of experimental study

The aim of experimental investigation is mainly to validate mathematical theoretical models and numerical models (discussed in Section 3.3.3). Another aim is to provide experimental support for parametric analysis study (introduced in Section 3.4). Since 2012, many experimental studies on the heat transfer and energy flow characteristics of TSCs have already carried out [14–17,19–21,25–29,32,33,38,39].

Belusko et al. [16] built an indoor experimental testing rig for the UTC with jet impingement, and carried out the thermal experiments involved subjecting the collector to the various flow rate and a constant irradiance. The maximum increase in thermal efficiency of UTC was

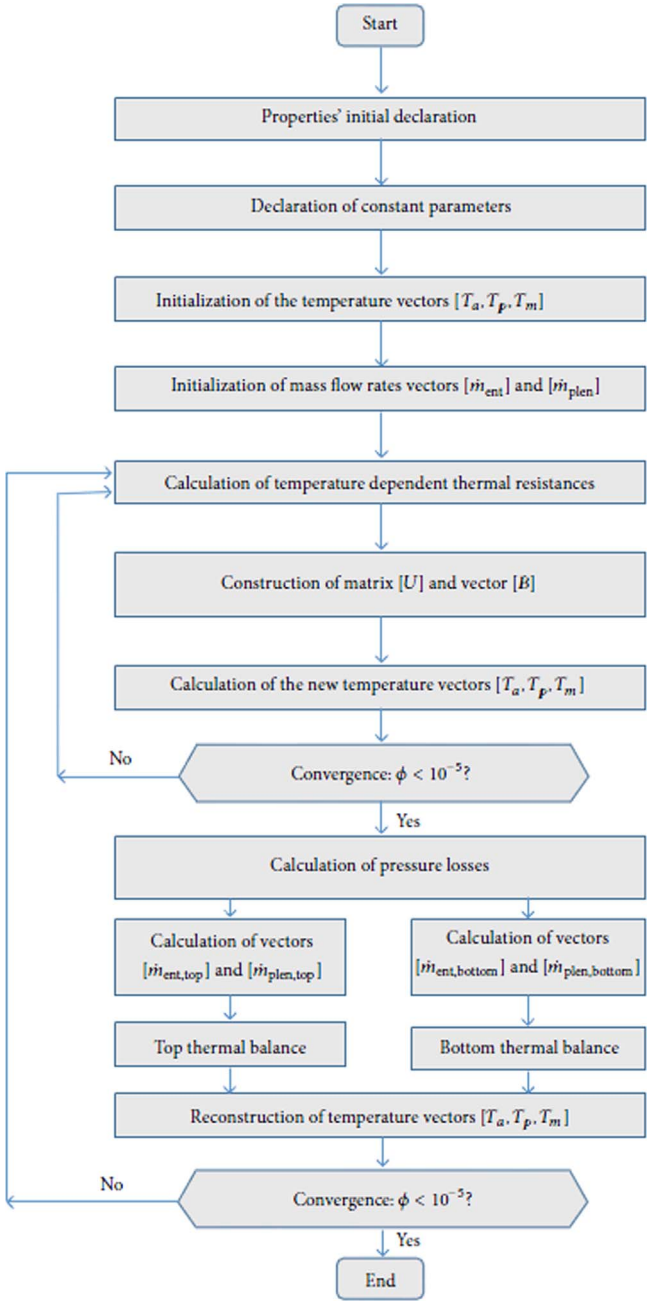

Fig. 3. Thermal network of corrugated UTCs (a) and UTCs with PV modules (b) from Li et al. [14].

found at x_n =80 with a mass flow rate of 0.046 kg/s/m, where the efficiency increased by 37% from 46% to 63%.

Vasan et al. [17] measured the velocity distribution on the UTC surface in a wind tunnel and performed a sensitivity study through the performance evaluation of UTC models based on diverse wind directions including 0°, 45° and 90°.

Croitoru et al. [19] carried out flow measurements based on PIV and visualizations, and temperature measurements using halide lamps for sun simulation in order to analyze the differences of the flow parameter for circular and lobed jets, and compare the baseline case with round perforations and the innovative cladding with lobed perforations, respectively.

Badache et al. [21] employed a full 3^4 factorial design-of-experiments method to optimize thermal performance of an UTC prototype. The optimized parameters included the hole diameter, absorber coating, irradiation and mass flow rate at three levels. The optimal combination of levels for the aforementioned four factors was able to provide the efficiency of collector up to 70–80%.

Greig et al. [25] conducted a detailed experimental investigation on the flow behavior characteristics over the corrugated geometry for different Reynolds numbers in a TSC system using PIV measurements. It was found that the strong turbulence occurs even at the Reynolds number lying within the conventional laminar domain.

Gholampour et al. [26] performed a detailed experimental study under different operating conditions and evaluated the prototype performance of PV/Thermal flat TSC system according to the energetic, equivalent thermal and exergetic efficiencies. This system was designed, constructed and tested under weather conditions in Kerman, Iran.

3.3. Numerical simulations

3.3.1. CFD simulation tools

Computational Fluid Dynamics (CFD) is the most popular methodology and advanced computational technique in recent two decades to predict 2D/3D airflow and heat transfer in and around active building envelopes with high temporal resolution. CFD is a powerful alternative tool for studying convective heat transfer on TSCs, eliminating difficulties combined with the precise control of the experimental conditions [22]. CFD models can provide the thermal and airflow field details as well as valuable insights for novel TSC designs which optimize the heat extraction [22].

The major CFD simulation tools available in the market are ANSYS/Fluent and ANSYS/CFX. Other CFD simulation tools include TASCflow 2.2, STAR-CCM+ etc [12,20].. GAMBIT and ICEM are employed for all geometry models and meshing. In addition, TRNSYS is another major simulation tool applied widely [50] for the simulation investigation of TSC. Lots of researchers have already applied commercial CFD code to investigate thermal performance of TSC in last five years [14,18,20,22,24,26,27,31].

Li et al. [14] predicted cavity exit air temperature, plate surface temperature with weather and design parameters and made energy prediction of UTCs with and without PV modules. Li et al. [18] in 2014 also investigated various important factors which affect the performance of corrugated UTCs with and without PV panels (BIPV/T). Tajdaran et al. [20] developed a comprehensive CFD model for TSC systems using STAR-CCM+ commercial software. It was found that HEE is at its highest value when TSC system operates at the lowest suction ratio with lowest wind speed. Li et al. [22] in 2013 analyzed the convective heat transfer processes for both flat and corrugated UTCs. It was concluded that the level of turbulence intensity is less significant than the presence of perforations in the approach flow for flat UTCs. But, for corrugated UTCs, the perforation dimensions play the less significant role in the system performance than incident turbulence intensity. Collins et al. [24] evaluated the effectiveness in the asymptotic region and heat loss due to wind in the starting region of an unglazed transpired solar collector with a trapezoidal corrugation. Gholampour et al. [26] developed a predictive model and validated and investigated the PV/Thermal flat transpired plate capabilities. Badache et al. [27] investigated thermal efficiency of a UTC for two plenum thickness (5 cm and 15 cm). The conclusion was drawn that both thermal efficiency of UTC and absorber plate effectiveness are relatively insensitive to the thickness of the plenum. Gao et al. [31] analyzed the heat transfer characteristic in UTC using CFD methodology. It is found that the hole pitch effect on heat transfer in UTC is important, while the hole diameter effect is less noticeable.

3.3.2. Turbulence models

It is very significant to select a suitable turbulence closure model to predict specific flow features and thermal fields for active building envelopes using CFD methodology. Li et al. evaluated the performance of five potentially suitable turbulence closure models including

Renormalization Normal Group k-ε (RNG k-ε), Standard k-ε, Shear Stress Transport k-ω (SST k-ω), Realizable k-ε and Reynolds Stress Model (RSM) applied in simulating both flat and corrugated UTCs [22]. Table 2 summarized the turbulence models for TSC simulation investigation since 2012. Observed from Table 2, the RNG k-ε is the most popular turbulence model selected by all those researchers.

Table 3 illustrates the comparison of all those five turbulence models for simulating UTCs. Seen from Table 3, it is found that the RNG k-ε has the best overall performance, which not only provides the most accurate and consistent results with economic computing cost, but also has more stable convergence. The Standard k-ε and SST k-ω models could have moderate accuracy, however, which are not as good as the RNG k-ε model. It is not recommended to use Realizable k-ε and RSM models for simulating UTCs due to their unsatisfactory overall performance e.g. inaccurate predicting results and higher computing cost [22].

3.3.3. Validation of numerical models

It is very necessary to validate the CFD numerical models and programs before it is extensively adopted for the scientific investigation [51–54]. Normally, the CFD simulation is validated against with experimental data under the same meteorological and operating conditions [26]. Li et al. [22] validated the CFD model based on two aspects including the airflow and thermal field for the flat UTC model and corrugated UTC model. The non-isothermal condition was considered for the flat UTC model because of limited available experimental data. The agreement of the plate surface temperature between CFD simulation results and experimental data are satisfactory due to error within 2 K; however, for the corrugated UTC model, both non-isothermal and isothermal cases have been taken into account and modeled. The agreement of stream-wise mean velocity and turbulent kinetic energy between the CFD results and experimental data is very good in the near wall region i.e. within 0.03 m [22].

Tajdaran et al. [20] performed several varieties of validation cases (15 cases) including diverse ambient air temperature, wind speed and angle, suction ratio, and vertical solar radiation, which imply that the sophisticated CFD model used in their work is able to deliver a realistic and accurate representation of the TSC system performance. In addition, it is found that CFD model is flexible in nature and well suitable to capture the effect of different climatic conditions [20]. (Fig. 4).

Authors used PIV data acquisition software to study complex fluid dynamics. It has been claimed that using CFD model and experimentation, a proposed geometry can increase the performance of conventional UTSC with almost 40% increase in thermal efficiency.

Hall et al. [50] carried out a two-fold model (TRNSYS) validation process for a novel flat cassette-panel TSC (CP-TSC) according to available experimental data from 95 days monitoring. The absorber plate temperature and plenum outlet temperature have been compared between simulation results and measured values. It was concluded that CP-TSC TRNSYS component is able to predict the daytime outlet air temperature (active outlet) with a high accuracy. The model is also good to predict the metal surface temperature when there is no flow through the perforations (bypass metal).

Collins et al. [24] validated their numerical model through comparing the simulation results of the absorber plate effectiveness with experimental values produced by Kutscher [9] and Van Decker et al. [47]. Their numerical simulation results slightly overestimate the effectiveness of the absorber plate at around 7%, although the difference appears in perforation shape.

Gholampour et al. [26] performed the validation of their numerical model for two PV/Thermal flat transpired plate systems (Fig. 5). One is with a PV panel (46% PV coverage) placed at the beginning of the transpired plate; another one is with two PV panels (92% PV coverage) located at the beginning and the end of the transpired plate. It is concluded that, for each validation case, there is a good agreement between the simulation and measured results for the mean PV panel temperature, outlet air temperature, and resistive load power.

Badache et al. [27] carried out various experimental measurements under different conditions including three air mass fluxes (0.0133, 0.0266 and 0.0411 kg/s/m^2), three irradiance levels (300, 450 and 600 W/m^2), and two plenum thicknesses (5 and 15 cm) in order to validate the CFD numerical models. In addition, the uncertainty of the experimental measurements have been also considered and investigated. The predicted collector efficiency from the numerical results lied within the uncertainty range for most of the measured efficiency. Particularly, for the cases of two plenum thicknesses, there was a good agreement between the measured values and simulation results at medium and high mass fluxes (0.0266 and 0.0411 kg/s/m^2). But, for the case of low mass flux (0.0133 kg/s/m^2), the numerical model over-predicted the experimental results. In addition, a minor difference was found for low (300 W/m^2) and medium (450 W/m^2) irradiance levels, however, an obvious difference appeared at high irradiance level (600 W/m^2). The reason of the disagreement is mainly due to a fact that the sky temperature is very hard to know accurately. Other disagreement reasons include temperature variations in the laboratory (estimated at ± 1.5 °C) and air movement resulted from the ventilation system.

Li et al. [14] measured the following parameters for the numerical model validation: the air temperature at the cavity exit, the surface temperature of four PV panels, and the representative temperature of ambient temperature; the airflow rate inside the cavity; the incident solar radiation; the approaching wind speed over the plate etc. It was concluded the model in the study could capture the trends and peaks very well. There was a satisfactory agreement between the model prediction and the experimental data for the cavity exit temperature in the configuration of lone UTC and for the PV surface temperature when the UTCs were combined with PV panels. Their corresponding RMSE are within 1 °C and 2 °C, respectively. However, the model prediction for the cavity exit temperature in the configuration of UTCs with PV panels is a little unsatisfactory, with the RMSE within 3 °C, because of the complex flow geometry.

Table 2
Summary of turbulence models for TSC simulation investigation since 2012.

Turbulence model	RNG k-ε	Standard k-ε	SST k-ω	Realizable k-ε	RSM	Others
Li et al. [14]	×					
Li et al. [18]	×					
Tajdaran et al. [20]				×		
Li et al. [22]	×	×	×	×	×	
Collins et al. [24]						Not mention
Gholampour et al. [26]	×					
Badache et al. [27]	×					
Gao et al. [31]						Not mention

Table 3
Comparison of turbulence models using CFD methodology [22].

Turbulence model	Accuracy	Computing cost	Performance	Convergence	Recommendation for simulating UTCs
RNG k-ε	Most accurate	Economic	Best overall	More stable	Yes
Standard k-ε	moderate	–	Good	More stable	Yes
SST k-ω	moderate	–	Acceptable	–	Yes
Realizable k-ε	inaccurate	–	Unsatisfactory	–	No
RSM	Bad	Much higher	Unsatisfactory	No (for non-isothermal)	No

3.4. Parametric study

The aim of parametric sensitivity analysis is to assess the dependence of diverse parameters in the heat transfer and energy characteristics of TSC [12]. The parametric sensitivity study has been already carried out by lots of researchers in past 20 years. Table 4 illustrates the various parametric study and the corresponding investigation results in recent five years.

There are many very significant parameters including perforation/hole diameter, pitch and pitch-to-diameter ratios, plate thickness, plenum thickness, width and depth, ambient and inlet air temperature, absorber porosity, solar radiation, airflow rate, approach flow velocity, (absorber coating) absorptivity and emissivity, wind angle and speed, incident turbulence intensity, corrugation collector wavelength, amplitude, crest and slope length, cavity width, PV panel width and height, distance between PV panels, time of the day, suction ratio, suction velocity ($m^3/s*m^2$) (or airflow rate), PV coverage percent, the location of PV panel, and air mass flux.

It is found that the effect of hole diameter and pitch on the thermal performance of GTC is less noticeable [30]. On the contrary, the effect of hole diameter and pitch on the HEE, effective efficiency and pressure drop is significant [15,33]. Increasing hole diameter and pitch will decrease HEE [33]. The reason resulting in completely different effects is depending on local climatic conditions, time and site constraints, and the interaction between different factors. Seen from Fig. 6, for an airflow rate of 72 $m^3/h*m^2$ and solar radiation of 900 W/m^2, changing the pitch from 12 to 24 mm (its corresponding change in perforation diameter from 0.80 to 1.55 mm) leads to a drop of 5.5 °C in the air temperature rise. The similar air temperature drops also appear in other solar radiation including 650 and 400 W/m^2 with a constant airflow rate [46]. Fig. 7 illustrates HEE as a function of collector pitch and perforation diameter. As mentioned before, observing from Fig. 7, increasing perforation diameter and collector pitch will decrease HEE [33].

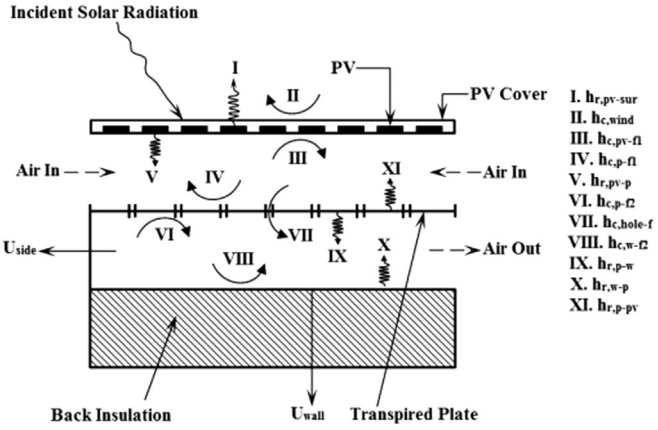

Fig. 5. Energy flow diagram of PV/Thermal flat transpired plate collector [26].

Thermal efficiency and the absorber plate effectiveness in UTC

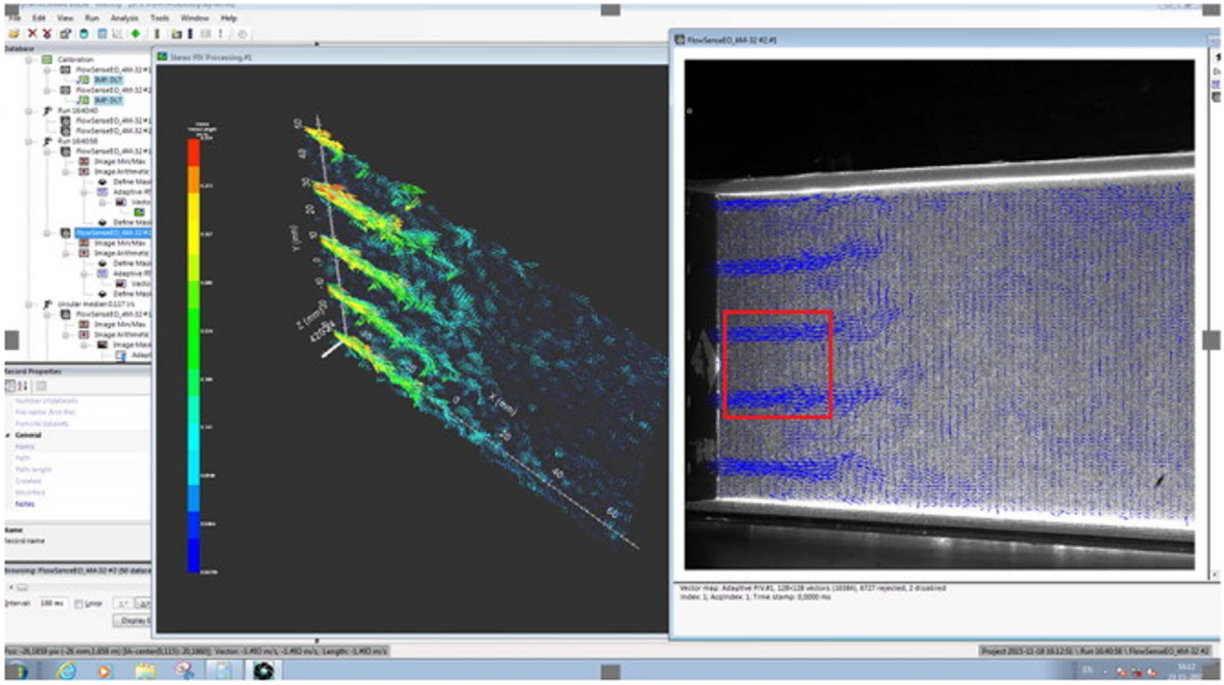

Fig. 4. PIV data acquisition software used by Tajdaran et al. [20].

Table 4
Comparison of parametric study and the corresponding investigation results.

Parameter	Study/Results
Effect of perforation/hole diameter and pitch	Effective efficiency increases with increasing perforation diameter and with decreasing pitch [15]. Perforation diameter and pitch have a stronger impact on pressure drop than on the heat collected [15]. Effect of hole diameter is not statistically significant (with > 95% certainty) [21]. The impact of hole diameter and hole pitch on the thermal performance of GTC is less obvious/noticeable [30]. The effect of hole pitch on heat transfer in UTC is noticeable [31]. The effect of hole diameter on heat transfer in UTC is less pronounced [31]. Increasing the hole pitch will reduce the HEE (Heat Exchanger Effectiveness) due to the decreasing HTC (Heat Transfer Coefficient) [33]. Increasing the hole diameter will decrease HEE and equivalent thermal efficiency [33].
Effect of plenum thickness and depth	Effective efficiency increases with shrinking plenum thickness [15]. The collector's thermal efficiency and the absorber plate effectiveness are relatively insensitive to the plenum thickness for UTC [27]. Efficiency of the TSC is moderately affected by the plenum thickness [32]. In the range of plenum depth, by increasing the plenum depth, higher equivalent thermal efficiency and thermal efficiency and second law efficiency for UTC occur [33].
Effect of ambient and inlet air temperature	Effective efficiency increases with decreasing inlet air temperature and with increasing ambient temperature [15]. An unfavorable effect on the PV/T TSC system performance for both first and second law efficiency with increasing ambient temperature [26]. Increasing the inlet air temperature will result in the decrease of equivalent thermal efficiency and second law efficiency [33]. The impact of external temperature on the temperature gain is slight [39].
Influence of solar radiation	Solar radiation ranges from 150 W/m^2 to 600 W/m^2 at 0° incidence angle (parallel flow) to the TSC is more effective than that at 67.5° incidence angle [20]. Increasing solar radiation has a desirable impact on the PV/T TSC system performance from both first and second law efficiencies [26]. The efficiency of UTCs is relatively insensitive to the irradiance [27]. The net heat loss from the absorber plate to the surroundings increases with increasing irradiance [27]. Solar radiation has large impact on exit air temperature and a minor impact on thermal efficiency of GTC [30]. Increasing irradiation has a negative effect on the collector efficiency for TTC [32]. With the increase of solar radiation, both the equivalent thermal efficiency and second law efficiency improve [33]. Increasing solar radiation will enhance the temperature rise [38]. Increasing incident solar irradiation, the temperature gain will linearly enhance [39].
Effect of airflow rate	Airflow rate has strong effect on exit air temperature [30]. Air mass flow rate (kg/s) has the greatest impact on the efficiency of TTC [32]. Increasing the airflow rate will reduce the temperature rise within the test range of 40 and 140 m^3/h/m^2 [38].
Effect of (absorber coating) absorptivity and emissivity	Effect of coating absorptivity is stronger than that of emissivity [15].
Effect of wind angle and speed	Winds with 45° incidence angle to the UTC have most significant impact on CHTC and HEE [17]. Increasing wind speeds from 1 m/s to 4 m/s will decrease both 'temperature rise' and 'surface temperature' [20]. Greater effect of wind speed on Heat Exchange effectiveness occurs/is found at higher suction ratios [20]. In theory, wind speed should have no influence on the calculated heat exchanger effectiveness [24]. Increasing wind velocity will increase heat loss and then decrease equivalent thermal efficiency and second law efficiency [33]. There is no effect of wind speed on the temperature rise per unit of solar radiation for the tested BPSC (Back-pass solar collector) within the range of 0.3 and 4 m/s [38].
Effect of incident turbulence intensity (TI)	Exterior Nu will increase with the turbulence intensity (TI), however, cavity exit air temperature and thermal efficiency will decrease with increasing TI, particularly when increasing wind speed and decreasing suction velocity [18].
Effect of corrugation collector wavelength	Increasing wavelength from 0.2 m to 1.2 m will increase $T_{collector}$ up to 10 °C and enhance energy efficiency up to three times higher [18].
Effect of corrugation collector amplitude	Effect of amplitude is hard to determine, since the collateral response to the slope length change is not able to be distinguished [18]. Decreasing amplitude will increase thermal efficiency for a reasonable assumption, since decreasing amplitude will decrease slope length [18].
Effect of corrugation collector crest and slope length	Effect of crest length on $T_{collector}$ is very minor [18]. Increasing crest length from 0.03 m to 0.11 m will enhance $T_{collector}$ within 0.2 °C [18]. Slope length has the most important effect on the thermal performance [18].
Effect of cavity width	Decreasing cavity width will cause a moderate increasing of $T_{collector}$ [18].
Effect of PV panel width and height	Effect of PV panel height is largest for UTCs with PV panels [18].
Effect of 'Time of the day'	TSCs deliver different operating temperatures dependent on time of day [20]
Effect of suction ratio (V_{suc}/V_{win})	Effect of suction ratio increases at lower wind speeds [20]. Increasing both suction ratio and wind speed result in decreasing heat exchange effectiveness [20].
Effect of suction velocity in m^3/s*m^2 (or airflow rate?)	Temperature behind the absorber decreases as the suction velocity increases [24]. For higher suction velocities, lower temperatures will cause higher heat transfer rates behind the absorber and lower heat exchanger effectiveness numbers for the absorber [24]. Increasing suction velocity will improve the first law efficiency but decrease the second law efficiency [26]. For GTC, the effect of suction velocity on thermal efficiency is not as noteworthy as that for UTC [30].

(continued on next page)

Table 4 *(continued)*

Parameter	Study/Results
	With increasing suction velocity, heat transfer in UTC is improved moderately [31]. Increasing suction velocity will enhance mass flow rate and heat transfer [33].
Effect of PV coverage percent	There is a significant impact of the PV coverage percent on the systems' (PV/T) performance [26]. Increasing coverage percent of PC has a positive impact on the second law efficiency but a negative impact on the first law efficiency [26].
Effect of the location of PV panel	There is a very small impact of the location of PV panel on the systems' (PV/T) performance [26].
Effect of air mass flux (kg/s/m^2)	With increasing air mass flux, the efficiency of UTCs improves [27]. With increasing air mass flux, the heat transfer predominance shifts progressively to the back-side of the absorber plate [27]. The net heat loss from the absorber plate to the surroundings increases with decreasing mass flux [27].

system are relatively insensitive to the plenum thickness [27]. However, efficiency of the TTC is moderately affected by the plenum thickness [32]. Sensitivity for the plenum depth to affect the efficiency of TSC is very significant. Increasing the plenum depth will improve equivalent thermal efficiency, thermal efficiency and second law efficiency [33].

Increasing inlet air temperature will reduce effective efficiency, equivalent thermal efficiency and second law efficiency [15,33]. Similar conclusions are also drawn that there is an unfavorable impact on the PV/T TSC system performance for both first and second law efficiency when increasing ambient temperature [26].

The effect of solar radiation on the collector system performance depends significantly on different types of TSC and incidence angle. For the PV/T TSC system, increasing solar radiation has a desirable impact on its performance from both first and second law efficiencies [26]. Similar conclusions are also drawn that the equivalent thermal efficiency, second law efficiency and temperature gain will enhance with increase in solar radiation [33,38,39]. The efficiency of UTC is relatively insensitive to the irradiance [27]. A minor effect of solar radiation on thermal efficiency of GTC is found [30], however, increasing irradiation has a negative effect on the collector efficiency for another TTC [32]. Fig. 8 shows exit air temperature as a function of solar radiation and airflow rate [46]. Seen from Fig. 8, increasing solar radiation for various airflow rates, all of the exit air temperature increase linearly.

Airflow rate has a strong effect on exit air temperature, the efficiency of TTC and temperature rise [30, 32, 38 and 46]. Fig. 9 shows collector efficiency as a function of airflow rate. Observing from Fig. 9, the collector efficiency increases exponentially with the airflow rate for various models [63].

With increase in wind speed, temperature rise and surface temperature will decrease [20], meanwhile, heat loss, equivalent thermal efficiency and second law efficiency increase [33]. On the contrary, there is no influence of wind speed on the calculated HEE in theory [24] and temperature rise per unit of solar radiation for the tested BPSC [38].

Increasing suction velocity will enhance the first law efficiency but decrease the second law efficiency [26], meanwhile, improve mass flow rate and heat transfer [31,33]. For GTC, the impact of suction velocity on thermal efficiency is not as significant as that for UTC [30].

The aforementioned effects of various parameters can be also categorized based on their similar characteristics as follows [12,18]. Among these, the most important significant parameters are the wind speed and suction velocity in TSCs [9,12,22,47,55–57], except the ambient air temperature and solar radiation [18].

- ***Effect of perforation geometry***: perforation/hole diameter and pitch, pitch-to-diameter ratios, hole shape and pattern [15,21,30,31,33].
- ***Effect of TSC configuration and its physical characteristics***: plate thickness, plenum thickness, width and depth [15,27,32,33], absorber porosity, (absorber coating) absorptivity and emissivity [15], PV coverage percent [26], corrugation collector wavelength, amplitude, crest and slope length [18], cavity width [18], PV panel width and height [18], distance between PV panels, color of coating.
- ***Effect of climatic conditions***: ambient and inlet air temperature [15,26,33,39], solar radiation [20,26,27,30,32,33,38,39], approach flow velocity, wind angle and speed [17,20,24,33,38], incident turbulence intensity [18], air mass flux [27].
- ***Effect of time and site constraints***: time of the day [20], the location of PV panel [26].

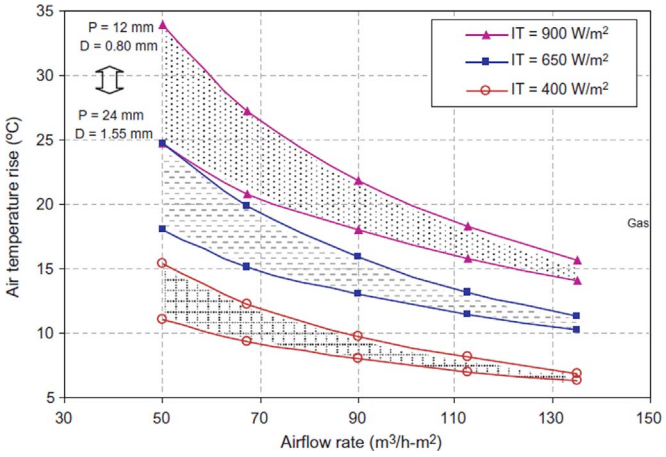

Fig. 6. Air temperature rise for various airflow rates under different pitch [46].

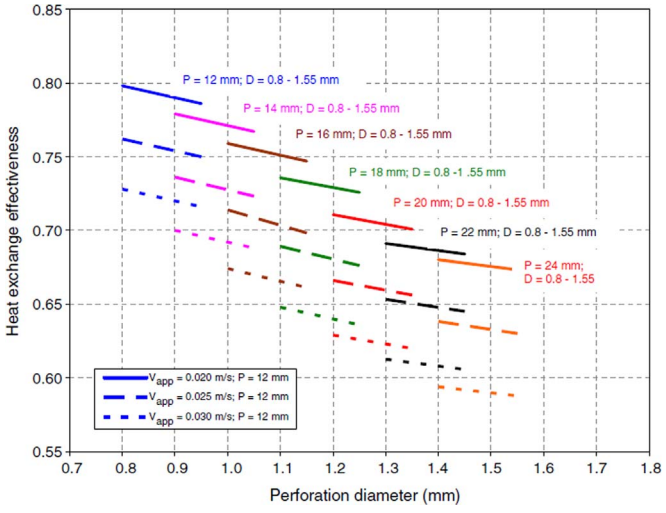

Fig. 7. Heat exchange effectiveness under different perforation diameter [46].

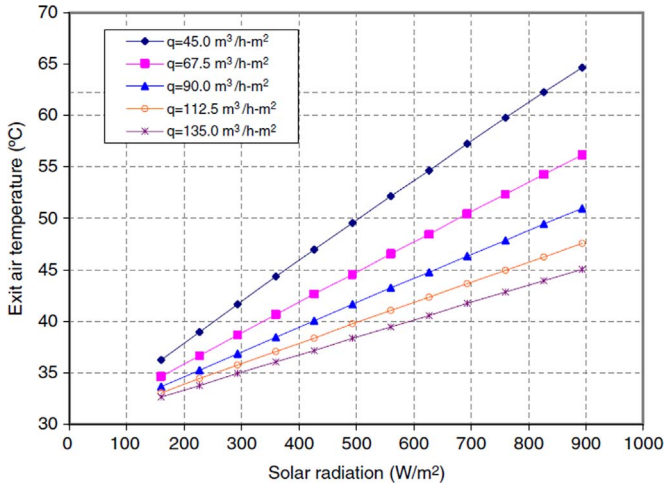

Fig. 8. Exit air temperature under solar radiation and airflow rate [46].

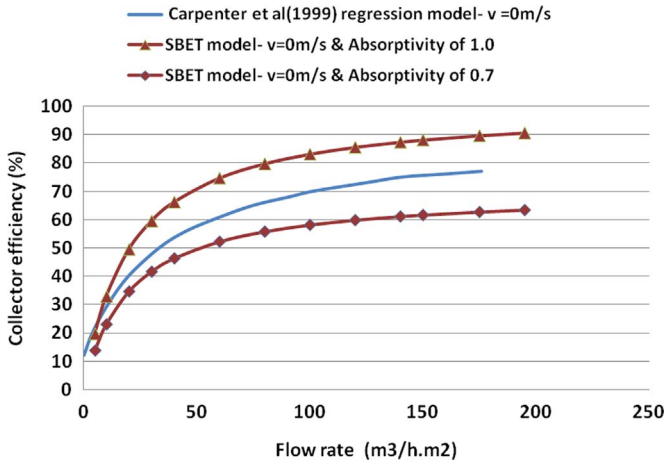

Fig. 9. Collector efficiency under airflow rate [63].

Table 5
Influence of temperature difference between outlet and ambient air temperature, solar irradiation and air mass flux on thermal efficiencies of TSCs [27,35,36].

Temperature difference (T_{out} - T_{amb}) in K	Thermal efficiency in %	Solar irradiation in W/m^2	Mass flux in kg/s per unit collector area
15	72	300	0.0133
10	84	300	0.0266
8	89	300	0.0411
25	72	450	0.0133
18	83	450	0.0266
12	89	450	0.0411
32	74	600	0.0133
20	83	600	0.0266
15	88	600	0.0411

- ***Effect of load characteristics***: airflow rate [30,32,38] or suction velocity (m^3/s*m^2) [24,26,30,31,33], suction ratio [20] in the system.

Table 5 shows the influence of temperature difference between outlet and ambient air temperature, solar irradiation and air mass flux on thermal efficiencies of TSCs [27,35,36]. Observed from Table 5, the most important factors affecting TSC thermal efficiency are temperature difference between outlet and ambient air temperature and air mass flux.

Since decreasing temperature difference between outlet and ambient air temperature or increasing air mass flux, when maintaining solar irradiance as a constant, will improve TSC thermal efficiency. Meanwhile, TSC thermal efficiencies reach the maximal value 89% when the temperature difference is minimal (8 K or 12 K for solar irradiance with 300 or 450 W/m^2, respectively) or air mass flux is maximal 0.0411 kg/s.

4. Conclusions and future work

In recent five years, various efficiency models of TSCs combined with PV modules have been developed not only from the perspective of energy, but also exergy. As advanced CFD numerical techniques develop, diverse turbulence models have been employed in analysis, evaluation and optimization on heat and airflow mass transfer, thermal efficiency, heat exchange efficiency, exergy efficiency, energy characteristics of TSCs integrated into other building services. The objective of this work has been met via following main valuable and scientific results found by intensive review of literature in past five years:

1) The most important significant parameters affecting TSC efficiency are the wind speed and suction velocity in TSCs. However, effects of various parameters on TSC efficiency are completely different, depending on local climatic conditions, time and site constraints, and the interaction between different factors.
2) Exergy analysis becomes more significant and helpful for a better design of TSC with PV/T system, since PV/Thermal flat transpired collectors generate both thermal and electrical energy. The second law efficiency represents the quality of useful energy gains, since the energy quality is very important for TSC with PV/T system.
3) The turbulence model of RNG k-ε has the best overall performance, which not only provides the most accurate and consistent results with economic computing cost, but also has more stable convergence, compared to standard k-ε, SST k-ω, Realizable k-ε and RSM.
4) The TSCs could be integrated with other building technologies e.g. PV modules, heat pump, mechanical ventilation with heat recovery, PCM etc., which will significantly enhance whole building energy efficiency.
5) There are many concepts for illustrating different point of view in TSC efficiency including the collector efficiency, effective efficiency, first law efficiency (energy efficiency), second law efficiency (exergy efficiency), equivalent thermal efficiency and instantaneous efficiency of the BPSC.

Current project of Active-LIVing Envelopes (ALIVE) from EPSRC [6,7] is now in the process of WP1 (Work Package) for investigating energy generation, storage and background research. WP2 for mathematical modelling using CFD and MATLAB and WP3 for experimental testing and electrical simulation will be carried out later on.

Acknowledgements

This research was fully supported by the Engineering and Physical Sciences Research Council - EPSRC, EP/N007557/1, for the project Active-LIVing Envelopes (ALIVE)). Underlying research material for this project can be accessed by contacting corresponding author and principal investigator of this project Dr. Ashish Shukla.

References

[1] Liu D, Zhao FY, Tang GF. Active low-grade energy recovery potential for building energy conservation. Renew Sustain Energy Rev 2010;14:2736–47.
[2] Anderson JE, Wulfhorst G, Lang W. Energy analysis of the built environment – A review and outlook. Renew Sustain Energy Rev 2015;44:149–58.
[3] Consumer-Appealing Low Energy Technologies for Building Retrofitting ('CALEBRE') grant on web ⟨http://gow.epsrc.ac.uk/NGBOViewGrant.aspx?GrantRef=EP/G000387/1⟩, Accessed on 20 March 2017.

[4] Carbon Plan ⟨https://www.gov.uk/government/uploads/system/uploads/attachment_data/file/47621/1358-the-carbon-plan.pdf⟩(2013) Accessed on 20 April 2017.
[5] Perez-Lombard L, Ortiz J, Pout C. A review on buildings energy consumption information. Energy Build 2008;40:394–8.
[6] Active Living Envelopes (ALIVE), grant on web. ⟨http://gow.epsrc.ac.uk/NGBOViewGrant.aspx?GrantRef=EP/N007557/1⟩ Accessed on 12 April 2017.
[7] Active Living Envelops, Project Website ⟨http://www.coventry.ac.uk/research/research-directories/current-projects/2016/active-living-envelopes-alive/⟩ Accessed on 18 April 2017.
[8] Kutscher CF, Christensen C, Barker G. Unglazed transpired solar collectors: an analytic model and test results. Proceedings of ISES Solar World Congress 1991, Denver, USA. Elsevier Science (2-1) 1245–1250; 1991.
[9] Kutscher CF. An investigation of heat transfer for air flow through low porosity perforated plates [Ph. D. Thesis]. Colorado, USA: Department of Mechanical Engineering, University of Colorado at Boulder; 1992.
[10] Gogakis C. Theoretical and experimental analysis of SolarWall technology. M. A. Sc. Thesis. School of Construction Management and Engineering, University of Reading, Berkshire, UK.
[11] Naveed AT, Kang EC, Lee EJ. Effect of unglazed transpired collector on the performance of a polycrystalline silicon photovoltaic module. J Sol Eng Trans ASME 2006;128:349–53.
[12] Shukla A, Nkwetta DN, Cho YJ, Stevenson V, Jones P. A state of art review on the transpired solar collector. Renew Sustain Energy Rev 2012;16:3975–85.
[13] RETScreen. Natural resources of Canada. Canmet Energy, ⟨http://www.retscreen.net/ang/home⟩; 2011.
[14] Li SW, Karava P, Currie S, Lin WE, Savory E. Energy modelling of photovoltaic thermal systems with corrugated unglazed transpired solar collectors – Part 1: model development and validation. Sol Energy 2014;102:282–96.
[15] Li XL, Li C, Li BJ. Net heat gain assessment on a glazed transpired solar air collector with slit-like perforations. Appl Therm Eng 2016;99:1–10.
[16] Belusko M, Saman W, Bruno F. Performance of jet impingement in unglazed air collectors. Sol Energy 2008;82:389–98.
[17] Vasan N, Stathopoulos T. Experimental study of wind effects on unglazed transpired collectors. Sol Energy 2014;101:138–49.
[18] Li SW, Karava P. Energy modelling of photovoltaic thermal systems with corrugated unglazed transpired solar collectors – Part 2: performance analysis. Sol Energy 2014;102:297–307.
[19] Croitoru CV, Nastase I, Bode FI, Meslem A. Thermodynamic investigation on an innovative unglazed transpired solar collector. Sol Energy 2016;131:21–9.
[20] Tajdaran S, Bonatesta F, Ogden R, Kendrick C. CFD modelling of transpired solar collectors and characterisation of multi-scale airflow and heat transfer mechanisms. Sol Energy 2016;131:149–64.
[21] Badache M, Halle S, Rousse D. A full 3^4 factorial experimental design for efficiency optimization of an unglazed transpired solar collector prototype. Sol Energy 2012;86:2802–10.
[22] Li SW, Karava P, Savory E, Lin WE. Airflow and thermal analysis of flat and corrugated unglazed transpired solar collectors. Sol Energy 2013;91:297–315.
[23] Li SW, Joe J, Hu JJ, Karava P. System identification and model-predictive control of office buildings with integrated photovoltaic-thermal collectors, radiant floor heating and active thermal storage. Sol Energy 2015;113:139–57.
[24] Collins MR, Abulkhair H. An evaluation of heat transfer and effectiveness for unglazed transpired solar air heaters. Sol Energy 2014;99:231–45.
[25] Greig D, Siddiqui K, Karava P. An experimental investigation of the flow structure over a corrugated waveform in a transpired air collector. Int J Heat Fluid Flow 2012;38:133–44.
[26] Gholampour M, Ameri M. Energy and exergy analyses of Photovoltaic/Thermal flat transpired collectors: experimental and theoretical study. Appl Energy 2016;164:837–56.
[27] Badache M, Rousse DR, Halle S, Quesada G. Experimental and numerical simulation of a two-dimensional unglazed transpired solar air collector. Sol Energy 2013;93:209–19.
[28] Greig D, Siddiqui K, Karava P. The influence of surface heating on the flow dynamics within a transpired air collector. Int J Heat Mass Transf 2013;56:390–402.
[29] Love CD, Shah SB, Grimes JL, Willits DW. Transpired solar collector duct for tempering air in North Carolina turkey brooder barn and swine nursery. Sol Energy 2014;102:308–17.
[30] Gao L, Bai H, Mao S. Potential application of glazed transpired collectors to space heating in cold climates. Energy Convers Manag 2014;77:690–9.
[31] Gao L, Bai H, Wu X. Numerical analysis of heat transfer in unglazed transpired collectors based on field synergy principle. Sol Energy 2013;95:336–44.
[32] Badache M, Halle S, Rousse DR, Quesada G, Dutil Y. An experimental investigation of a two-dimensional prototype of a transparent transpired collector. Energy Build 2014;68:232–41.
[33] Rad HM, Ameri M. Energy and exergy study of unglazed transpired collector-2stage. Sol Energy 2016;132:570–86.
[34] Shams SMN, Mc Keever M, Mc Cormack S, Norton B. Design and experiment of a new solar air heating collector. Energy 2016;100:374–83.
[35] Colangelo G, Favale E, Miglietta P, de Risi A. Innovation in flat solar thermal collectors: a review of the last ten years experimental results. Renew Sustain Energy Rev 2016;57:1141–59.
[36] Badache M, Rousse D, Halle S, Quesada G, Dutil Y. Experimental and two-dimensional numerical simulation of an unglazed transpired solar air collector. Energy Procedia 2012;30:19–28.
[37] Zhang T, Tan Y, Zhang X, Li Z. A glazed transpired solar wall system for improving indoor environment of rural buildings in northeast China. Build Environ 2016;98:158–79.
[38] Paya-Marin MA, Lim JBP, Chen JF, Lawson RM. Large scale test of a novel back-pass non-perforated unglazed solar air collector. Renew Energy 2015;83:871–80.
[39] Semenou T, Rousse DR, Le Lostec B, Nouanegue HF, Paradis PL. Mathematical modelling of dual intake transparent transpired solar collector, Mathematical Problems in Engineering; 2015.
[40] Athienitis AK, Bambara J, O'Neill B, Faille J. A prototype photovoltaic/thermal system integrated with transpired collector. Sol Energy 2011;85:139–53.
[41] Gupta MK, Kaushik SC. Performance evaluation of solar air heater for various artificial roughness geometries based on energy, effective and exergy efficiencies. Renew Energy 2009;34:465–76.
[42] Petela R. Exergy of heat radiation. J Heat Transf 1964;86:187–92.
[43] Bahrehmand D, Ameri M, Gholampour M. Energy and exergy analysis of different solar air collector systems with forced convection. Renew Energy 2015;83:1119–30.
[44] Coventry JS, Lovegrove K. Development of an approach to compare the 'value' of electrical and thermal output from a domestic PV/thermal system. Sol Energy 2003;75:63–72.
[45] Hottel HC, Whillier W. Evaluation of flat plate solar collector performance. Transaction of Conference for Use of Solar Energy Thermal Processes, Tuscon AZ; 1955.
[46] Leon MA, Kumar S. Mathematical modelling and thermal performance analysis of unglazed transpired solar collectors. Sol Energy 2007;81:62–75.
[47] Van Decker GWE, Hollands KGT, Brunger AP. Heat-exchange relations for unglazed transpired solar collectors with circular holes on a square or triangular pitch. Sol Energy 2001;71:33–45.
[48] Kutscher CF. Heat exchange effectiveness and pressure drop for air flow through perforated plates with and without crosswind. J Heat Transf 1994;116:391–9.
[49] Skoplaki E, Palyvos JA. On the temperature dependence of photovoltaic module electrical performance: a review of efficiency/power correlations. Sol Energy 2009;83:614–24.
[50] Hall R, Kendrick C, Lawson MR. Development of a cassette-panel transpired solar collector. ICE Energy 2013;16:32–41.
[51] Wang Y, Zhao FY, Kuckelkorn J, Liu D, Liu J, Zhang JL. Classroom energy efficiency and air environment with displacement natural ventilation in a passive public school building. Energy Build 2014;70:258–70.
[52] Wang Y, Zhao FY, Kuckelkorn J, Spliethoff H, Rank E. School building energy performance and classroom air environment implemented with the heat recovery heat pump and displacement ventilation system. Appl Energy 2014;114:58–68.
[53] Wang Y, Zhao FY, Kuckelkorn J, Liu D, Liu LQ, Pan XC. Cooling energy efficiency and classroom air environment of a school building operated by the heat recovery air conditioning unit. Energy 2014;64:991–1001.
[54] Wang Y, Zhao FY, Kuckelkorn J, Li XH, Wang HQ. Indoor air environment and night cooling energy efficiency of a southern German passive public school building operated by the heat recovery air conditioning unit. Energy Build 2014;81:9–17.
[55] Golneshan AA. Forced convection heat transfer from low porosity slotted transpired plates [Ph. D. Thesis]. Waterloo, Canada: Department of Mechanical Engineering, University of Waterloo; 1994.
[56] Bambara J. Experimental study of a façade-integrated photovoltaic/thermal system with unglazed transpired collector [M. A. Sc. Thesis]. Montreal, Canada: Department of Building, Civil and Environmental Engineering, Concordia University; 2012.
[57] Li SW, Karava P. Evaluation of turbulence models for airflow and heat transfer prediction in BIPV/T systems optimization. Energy Procedia 2012;30:1025–34.
[58] Ozgen F, Esen M, Esen H. Experimental investigation of thermal performance of a double-flow solar air heater having aluminium cans. Renew Energy 2009;11(34):2391–8.
[59] Esen H, Ozgen F, Esen M, Sengur A. Modelling of a new solar air heater through least-squares support vector machines. Expert Syst Appl 2009;7(36):10673–82.
[60] Esen H, Ozgen F, Esen M, Sengur A. Artificial neural network and wavelet neural network approached for modelling of a solar air heater. Expert Syst Appl 2009;36(8):11240–8.
[61] Esen H, Esen M, Ozsolak O. Modelling and experimental performance analysis of solar-assisted ground source heat pump system. J Exp Theor Artif Intell 2017;29(1):1–17.
[62] Esen M, Yuksel T. Experimental evaluation of using various renewable energy sources for heating a greenhouse. Energy Build 2013;65:340–51.
[63] Cho YJ, Shukla A, Nkwetta DN, Jones P. Thermal modelling and parametric study of transpired solar collector. CIBSE ASHRAE Technical Symposium, Imperial College London, UK, April 18 – 19; 2012.